

Nonequilibrium thermodynamics in the strong coupling and non-Markovian regime based on a reaction coordinate mapping

Philipp Strasberg¹, Gernot Schaller¹, Neill Lambert², and Tobias Brandes¹

¹ *Institut für Theoretische Physik,
Technische Universität Berlin,
Hardenbergstr. 36, D-10623 Berlin, Germany*
² *CEMS, RIKEN, Saitama, 351-0198, Japan*

We propose a method to study the thermodynamic behaviour of small systems beyond the weak coupling and Markovian approximation. This method – based on a reaction coordinate mapping – is general in the sense that it can be applied to an arbitrary (quantum or classical and even time-dependent) system coupled linearly to an arbitrary number of harmonic oscillator reservoirs. The core of the method relies on an appropriate identification of a part of the environment (the reaction coordinate), which is subsequently included as a part of the system. This supersystem is then treated within the weak coupling and Markovian approximations, ensuring that we obtain a consistent thermodynamic picture. We demonstrate the power of this concept by showing that non-Markovian effects can significantly enhance the steady state efficiency of a three-level-maser heat engine, even in the regime of weak system-bath coupling. Furthermore, we show for a single electron transistor coupled to vibrations that our method allows one to justify the widely used polaron transformation.

I. INTRODUCTION

Classical thermodynamics is a weak coupling theory in the sense that boundary or surface terms of the system are negligible compared to its bulk or volume properties. This becomes particularly apparent in Maxwell’s colloquial description of the zeroth law of thermodynamics: “All heat is of the same kind” [1]. By this statement he meant that the laws governing the transformation of heat are independent of how we put two different systems into contact – a conclusion which obviously holds only if the influence of this contact can be neglected. Other implications of the weak coupling approximation are, for instance, the extensiveness of internal energy or entropy if two subsystems are put into contact [2].

While the weak coupling approximation can be well justified for macroscopic systems due to simple geometric arguments (the surface to volume ratio usually decreases with increasing volume), it is harder to justify in the opposite limit when the volume of the system becomes very small. This, however, is the regime where quantum and stochastic effects dominate. Then, in order to link microscopic theory with thermodynamics, one usually starts with a Hamiltonian of the form

$$H = H_S + H_E + H_I \quad (1)$$

where H_S (H_E) is the Hamiltonian of the system (environment) and H_I describes their interaction (the “contact”). Assuming that the coupling H_I is small, one then performs a perturbative expansion up to second order in H_I which (under the additional assumption that the environment is memory-less) yields a closed and Markovian evolution equation for the system density matrix ρ_S , known as a (quantum) master equation (ME). We note that similar assumptions are needed to derive (classical) Fokker-Planck or Langevin equations. MEs derived this

way can then be shown to have a transparent thermodynamic interpretation [3–5] and they provide the work horse for the field of quantum and stochastic thermodynamics, see Refs. [6–10] for recent reviews.

However, many interesting physical effects cannot be captured with such a ME approach and thus, quantum and stochastic thermodynamics is still restricted to a small regime of applicability. Consequently, many groups have started to look at thermodynamics in the strong coupling and non-Markovian regime [11–36]. Though these works present important theoretical cornerstones, they are still far away from providing a satisfactory extension of thermodynamics beyond the weak coupling limit. In particular, if one wishes to address the performance of a steadily working heat engine, the general results derived in Refs. [11–20] are not of great help because they either focus on integrated changes of thermodynamic values (e.g., the total heat exchanged in a finite time instead of the *rate* of heat exchange) and additionally rely on an initially decorrelated system-environment state [11–13] and/or coupling only to a single thermal reservoir [11, 13–16]; or they remain very formal [17–20]. Furthermore, model-specific studies are either based on simple or exactly solvable models from the field of quantum transport [21–24] and quantum Brownian motion [25–27], or spin-boson models [28–30] often in combination with specific transformations applicable only to special Hamiltonians (polaron transformations) [29, 31–34]; or the investigations are restricted to numerical studies [35], or they require additional assumptions such as an alternating coupling and decoupling of the system from the environment [36].

The goal of this paper is to close the gap between the general results, which are often hard to apply in practice, and studies restricted to overly-specific models. Here, we propose a framework which allows to carry over all concepts known from the weak coupling regime of thermody-

namics to the strong coupling and non-Markovian regime (we will in fact see that strong coupling is easier to treat than non-Markovianity). Our framework is general in the sense that it can be applied to an *arbitrary* (quantum or classical¹ and even driven) system coupled linearly to an arbitrary number of harmonic oscillator heat baths. Thus, apart from not being able to treat fermionic reservoirs at the moment, we capture many relevant situations encountered in the study of small-scale engines.

To achieve this, we will identify a collective degree of freedom in the reservoir which is then incorporated into the description of the system. This collective degree of freedom is known as a *reaction coordinate* (RC) [37], which will capture non-Markovian and strong coupling effects. For this “supersystem” (original system plus RC) we will derive the ME as usual allowing for a transparent interpretation of the laws of thermodynamics. We note that a complementary analysis of non-Markovian effects in thermodynamics, employing the RC mapping, appears in a related work by Newman *et al.* [38]. Apart from the thermodynamic applications we propose here, it has been shown that such a RC mapping can provide a very accurate method to investigate the non-Markovian behaviour of open quantum systems for a variety of problems [39–42]. Even more generally, it is possible to apply this method iteratively by including several RCs and in this way one can prove that every non-Markovian environment can be mapped to a Markovian one [43–45].

Apart from adapting this general method to treat heat engines in the strong coupling and non-Markovian regime, we also consider concrete applications. In particular, we find that non-Markovian effects can significantly enhance the steady state efficiency even in the weak coupling regime; a result which – to the best of our knowledge – has not been found before. In addition, we also investigate the relation between our method and the widely used polaron transformation, showing that the RC framework provides a means to justify particular polaron transformed ME (PME), and reduces to it under special circumstances.

Outline: We will start by introducing the general technique of the RC mapping in Sec. II as far as it is needed to make the present treatment self-consistent. After having established this tool, we will present the general thermodynamic framework based on it in Sec. III. Particular applications to devices working out of equilibrium then follow in Sec. IV (efficiency study of a maser heat engine in the non-Markovian regime) and Sec. V (a single electron transistor (strongly) coupled to vibrations). Final remarks about the range of validity, open problems and the thermodynamic interpretation of the method are given in Sec. VI.

¹ The notation we are using is adapted to the quantum mechanical situation but all transformations carry over to the classical situation, too.

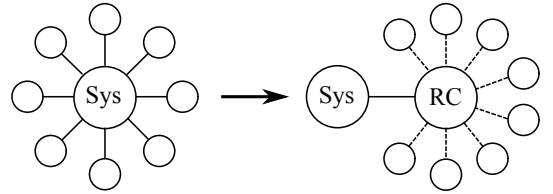


FIG. 1: Sketch of the RC mapping. Before the mapping (left figure) the system can be visualized as being coupled to a large number of harmonic oscillators, see Eq. (2). After the mapping (right figure) the system couples to the RC only, but in turn the RC is coupled to a large number of residual oscillators as described by the Hamiltonian (17).

II. REACTION COORDINATE MAPPING

We consider an arbitrary system with Hamiltonian $H_S(t)$ coupled linearly via some system operator s to a bath of harmonic oscillators (the coupling to several baths follows straightforwardly from this treatment, see next section). The total Hamiltonian is assumed to have the typical Brownian motion form [46, 47]

$$H = H_S(t) + \frac{1}{2} \sum_k \left[p_k^2 + \omega_k^2 \left(x_k - \frac{c_k}{\omega_k^2} s \right)^2 \right] \quad (2)$$

with mass-weighted positions x_k and momenta p_k of the bath fulfilling $[x_k, p_l] = i\delta_{kl}$ (we set $\hbar \equiv 1$ throughout). It is worth to point out that the completion of the square is important for a number of reasons, e.g., to guarantee a thermodynamically stable Hamiltonian *for all* coupling strengths c_k [48]. In the derivation of MEs one often neglects the quadratic system “renormalization” term $\frac{1}{2} \sum_k \frac{c_k^2}{\omega_k^2} s^2$ from the beginning, though its contribution is, in principle, of the same order as the Lamb shift term.

An important result of the microscopic theory of Brownian motion is that the effect of the bath on the system can be captured solely by one special function known as the spectral density (SD) of the bath:

$$J_0(\omega) \equiv \frac{\pi}{2} \sum_k \frac{c_k^2}{\omega_k} \delta(\omega - \omega_k). \quad (3)$$

The SD is a positive function for $\omega > 0$ and must fulfill $J_0(\omega) \rightarrow 0$ for $\omega \rightarrow 0$ and $\omega \rightarrow \infty$.

Now, the spirit of the RC method is to define the interaction with the collective degrees of the freedom of the bath as one new coordinate: the reaction coordinate X_1 (see Fig. 1). Hence, we seek a transformation which maps

$$\sum_k c_k x_k = \lambda_0 X_1 \quad (4)$$

where λ_0 is an unspecified parameter so far. More formally, we perform a normal mode transformation of the form

$$\mathbf{X} = \Lambda \mathbf{x}, \quad \mathbf{P} = \Lambda \mathbf{p}. \quad (5)$$

Here, we used a vector notation for the collection of original and transformed bath coordinates and momenta, e.g., $\mathbf{x} = (x_1, \dots, x_k, \dots, x_N)^T$ describes the original bath coordinates. For definiteness we considered a finite number of N bath oscillators (having the limit $N \rightarrow \infty$ in mind). Furthermore, Λ is an orthogonal $N \times N$ matrix, i.e., $\Lambda^{-1} = \Lambda^T$, which guarantees that $[X_k, P_l] = i\delta_{kl}$. Thus, Λ has $\frac{N(N-1)}{2}$ independent components which are fixed by the requirement that the collection of residual bath oscillators (i.e., all oscillators except the RC itself) is of normal form. This leads to

$$\sum_k \omega_k^2 \Lambda_{lk} \Lambda_{mk} = \delta_{lm} \Omega_l^2 \quad (6)$$

for $l \neq 1$ and $m \neq 1$ and allows us to map the Hamiltonian (2) to

$$\begin{aligned} H' = & H_S(t) + \frac{\delta\Omega_0^2}{2} s^2 - \lambda_0 s X_1 + \frac{1}{2} (P_1^2 + \Omega_1^2 X_1^2) \\ & - X_1 \sum_{k \neq 1} C_k X_k + \frac{1}{2} \sum_{k \neq 1} (P_k^2 + \Omega_k^2 X_k^2). \end{aligned} \quad (7)$$

Here, we used $\Lambda_{1k} = \lambda_0^{-1} c_k$ which follows from Eq. (4). Furthermore, we defined $\Omega_1^2 \equiv \sum_k \omega_k^2 \Lambda_{1k}^2$ and $C_k \equiv -\sum_l \omega_l^2 \Lambda_{kl} \Lambda_{k1}$. Finally, the system gets renormalized due to $\delta\Omega_0^2 \equiv \sum_k \omega_k^{-2} c_k^2$ and from $[X_1, P_1] = i$ we can deduce that $\lambda_0^2 = \sum_k c_k^2$.

At this point we can already recognize an important property of the mapping. Suppose that we scale the coupling coefficients c_k by $c_k \mapsto \alpha c_k$ for some $\alpha \in \mathbb{R}$. Then, the only parameters influenced by this will be λ_0 and $\delta\Omega_0$, i.e., all information about the overall original system bath coupling strength is captured in the system RC coupling and a system renormalization term. The remaining terms, especially the new coupling coefficients C_k , are *independent* of the initial coupling strength α .

Now, the crux of the matter is that we do not have to determine Λ directly; instead, the normal mode transformation can be fully fixed by knowledge of the SD $J_0(\omega)$ only [37]. To see this we first of all note that all relevant quantities of the system and RC itself can be expressed in terms of the original SD as follows:

$$\delta\Omega_0^2 = \frac{2}{\pi} \int_0^\infty d\omega \frac{J_0(\omega)}{\omega}, \quad (8)$$

$$\lambda_0^2 = \frac{2}{\pi} \int_0^\infty d\omega \omega J_0(\omega), \quad (9)$$

$$\Omega_1^2 = \frac{2}{\pi \lambda_0^2} \int_0^\infty d\omega \omega^3 J_0(\omega). \quad (10)$$

The effect of the residual environment on the system and RC is itself captured by the new SD

$$J_1(\omega) \equiv \frac{\pi}{2} \sum_k \frac{C_k^2}{\Omega_k} \delta(\omega - \Omega_k) \quad (11)$$

and the remaining task is to relate $J_0(\omega)$ to $J_1(\omega)$. We will here use the prescription given by Martinazzo *et*

al. [44] who have shown the following relation under reasonable mild conditions²

$$J_1(\omega) = \frac{\lambda_0^2 J_0(\omega)}{|W_0^+(\omega)|^2}. \quad (12)$$

For completeness we will present a derivation of this result in Appendix A. Similar methods to link the SDs can be found in Refs. [37, 40, 43, 45]. In Eq. (12), $W_0(z)$ denotes the Cauchy transform of $J_0(\omega)$ given by

$$W_0(z) \equiv \frac{1}{\pi} \int_{-\infty}^{\infty} d\omega \frac{J_0(\omega)}{\omega - z} \quad (13)$$

[we extended $J_0(\omega)$ to negative values of ω via $J_0(-\omega) = -J_0(\omega)$] and we introduced the notation

$$W_0^+(\omega) \equiv \lim_{\epsilon \searrow 0} W_0(\omega + i\epsilon) \quad (\omega \in \mathbb{R}). \quad (14)$$

Furthermore, one can also show that (see Ref. [44] or Appendix A again)

$$\frac{\lambda_0^2}{\delta\Omega_0^2} = \Omega_1^2 - \delta\Omega_1^2, \quad (15)$$

where we denoted the frequency renormalization term of the RC by

$$\delta\Omega_1^2 = \sum_k \frac{C_k^2}{\omega_k^2} = \frac{2}{\pi} \int_0^\infty d\omega \frac{J_1(\omega)}{\omega}. \quad (16)$$

Relation (15) allows us to rewrite the Hamiltonian (7) in a Brownian motion form [41]

$$\begin{aligned} H' = & H_S(t) + \frac{1}{2} \left[P_1^2 + \frac{\lambda_0^2}{\delta\Omega_0^2} \left(X_1 - \frac{\delta\Omega_0^2}{\lambda_0} s \right)^2 \right] \\ & + \frac{1}{2} \sum_k \left[P_k^2 + \Omega_k^2 \left(X_k - \frac{C_k}{\Omega_k^2} X_1 \right)^2 \right], \end{aligned} \quad (17)$$

which makes its thermodynamic stability evident. Hence, the *physical* frequency of the RC is not given by Ω_1 but by the square-root of Eq. (15).

Finally, we note that the power of the RC mapping also comes from the fact that it can be applied iteratively. This then yields a chain of RCs where the last one is coupled to a residual environment. Remarkably, the relation between the SDs, Eq. (12), still carries over to this situation (replacing the index 0 by n and the index 1 by $n+1$ where n labels the different RCs) and also all other parameters can be defined in terms of the SD as in Eqs. (8) to (10). This was shown in Refs. [43–45] and Refs. [44, 45] also show that in the limit of many RCs the sequence $J_n(\omega)$ of SDs is guaranteed to converge to a

² $J_0(\omega)$ should be continuous and strictly positive for $\omega \in (0, \omega_R)$ and zero for $\omega \geq \omega_R$ where ω_R denotes a cutoff frequency [44].

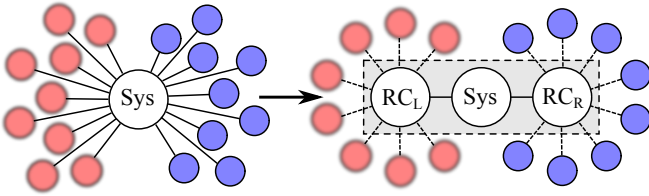


FIG. 2: (color online). Sketch of a system coupled to a hot reservoir (red, blurred oscillators) and a cold reservoir (blue oscillators). After the mapping we have, as an example, included one RC for each reservoir to account for non-Markovian and strong coupling effects. Note, however, that we do not have to include a RC if the reservoir is weakly coupled and Markovian, or we might have to include two or more RCs in case of strong non-Markovianity. After the mapping we then treat the system and RCs as one new system as indicated by the shaded grey box.

Markovian one.³ Thus, already at this time we can conclude that arbitrary strong coupling effects can be effectively captured by including only *one* RC (a more critical discussion of this point is shifted to Sec. VI) while strong non-Markovianity might require several RCs.

III. NONEQUILIBRIUM THERMODYNAMICS WITHIN THE REACTION COORDINATE FRAMEWORK

We now imagine the situation where our system is coupled to several reservoirs labeled by ν and where the time-dependent driving is responsible for work extraction and injection. The obvious generalisation of the Hamiltonian (2) to this situation is

$$H = H_S(t) + \frac{1}{2} \sum_{k,\nu} \left[p_{k\nu}^2 + \omega_{k\nu}^2 \left(x_{k\nu} - \frac{c_{k\nu}}{\omega_{k\nu}^2} s_\nu \right)^2 \right] \quad (18)$$

where the coupling to reservoir ν is mediated by the system operator s_ν which might be all different for different ν . A sketch of a possible scenario is shown in Fig. 2. We can then decide to include zero, one or several RCs for each reservoir depending on the coupling strength and the shape of the SD. Again, all what we need to know for this mapping are the SDs $J_0^{(\nu)}(\omega)$ for each reservoir ν . The same transformations as introduced in Sec. II will carry over in exactly the same way to the situation

of multiple reservoirs. It is in particular worth pointing out that each RC mapping is a unitary transformation *only* on the Hilbert space of bath ν , i.e., it leaves the system part and all other baths fully untouched. This feature allows us to really present a *general* thermodynamic framework valid for any system, which is coupled to its environment in the prescribed way.

After having included a sufficient number of RCs, the next step is to define a new “supersystem” consisting out of the original system and all RCs. The idea is then to treat this supersystem within the standard Born-Markov-secular (BMS) approximation [40, 42], assuming that the bath of the residual oscillators is in thermal equilibrium, and to derive a Markovian ME for the supersystem. This ME then has a transparent thermodynamic interpretation, as we will review below for reasons of consistency. It is especially worth pointing out that already including one RC can give remarkable numerical results in agreement with the formally exact hierarchical equations of motion method, as it was recently shown by Iles-Smith *et al.* [40, 42].

The standard framework of quantum thermodynamics starts with a microscopically derived ME of the form [4–6, 8–10]

$$\frac{d}{dt} \rho(t) = -i[H'_S(t), \rho(t)] + \sum_{\nu} \mathcal{L}^{(\nu)}(t) \rho(t). \quad (19)$$

Here, $\rho(t)$ denotes the density matrix and $H'_S(t)$ the Hamiltonian of the supersystem, i.e., the system *and* RCs. The time-dependence of $H'_S(t)$ might result from an initial time-dependence of $H_S(t)$. For example, in case of a single RC we have [see Eq. (17)]

$$H'_S(t) = H_S(t) + \frac{1}{2} \left[P_1^2 + \frac{\lambda_0^2}{\delta\Omega_0^2} \left(X_1 - \frac{\delta\Omega_0^2}{\lambda_0} s \right)^2 \right]. \quad (20)$$

Furthermore, the dissipators or thermal generators $\mathcal{L}^{(\nu)}(t)$ are of Lindblad form [52] and fulfill local detailed balance, i.e.,

$$\mathcal{L}^{(\nu)}(t) e^{-\beta_\nu H'_S(t)} = 0 \quad (21)$$

where β_ν is the temperature of reservoir ν .⁴ We remark that, strictly speaking, a ME of the form (19) can only be derived for a slow time-dependence of $H_S(t)$. However, using techniques from Floquet theory it is also possible to derive a ME for (strong) periodic driving [52] with a similar thermodynamic interpretation [8, 10, 53]. For an arbitrary driving $H_S(t)$ there is no guarantee to find a simple ME for the system, but a thermodynamic analysis

³ In the theory of Brownian motion, Markovian behaviour is ensured by an Ohmic SD which scales linearly with ω up to a high enough frequency cutoff ω_R and then falls off to zero [46]. We stress, however, that the correct definition of non-Markovianity in the quantum mechanical context is non-trivial, may not be guaranteed by this condition alone, and is under much debate at the moment, see, e.g., [49–51]

⁴ If we also allow for particle transport by coupling the system to a particle reservoir with chemical potential μ_ν , we have the relation $\mathcal{L}^{(\nu)}(t) e^{-\beta_\nu [H'_S(t) - \mu_\nu N'_S]} = 0$ instead where N'_S is the particle number operator of the supersystem.

can be still carried out [54] (see also the general treatment [12]).

We now define the internal energy and entropy of the supersystem via

$$E(t) \equiv \text{tr}\{H'_S(t)\rho(t)\}, \quad S(t) \equiv -\text{tr}\{\rho(t) \ln \rho(t)\}. \quad (22)$$

The first law of thermodynamics then acquires the form

$$\frac{d}{dt}E(t) = \dot{W}(t) + \sum_{\nu} \dot{Q}^{(\nu)}(t) \quad (23)$$

where we identified the rate of work (power) *done on* the supersystem and the heat flow coming *from* reservoir ν as⁵

$$\dot{W}(t) \equiv \text{tr} \left\{ \rho(t) \frac{d}{dt} H_S(t) \right\}, \quad (24)$$

$$\dot{Q}^{(\nu)}(t) \equiv \text{tr} \left\{ H'_S(t) \mathcal{L}^{(\nu)}(t) \rho(t) \right\}. \quad (25)$$

In Eq. (24) we used that $\frac{d}{dt} H'_S(t) = \frac{d}{dt} H_S(t)$. The second law stipulates that the rate of entropy production $\dot{S}_i(t)$ is always positive,

$$\dot{S}_i(t) = \frac{d}{dt} S(t) - \sum_{\nu} \beta_{\nu} \dot{Q}^{(\nu)}(t) \geq 0. \quad (26)$$

It is possible to prove Eq. (26) by use of Spohn's inequality stating that [3]

$$-\text{tr} \left\{ \left[\mathcal{L}^{(\nu)}(t) \rho(t) \right] \left[\ln \rho(t) - \ln \rho_{\text{eq}}^{(\nu)} \right] \right\} \geq 0 \quad (27)$$

for every ν and $\rho_{\text{eq}}^{(\nu)} \equiv e^{-\beta_{\nu} H'_S(t)} / Z_{\nu}$. By summing Eq. (27) over ν we obtain the second law.

Finally, if the system is undriven it will eventually reach a steady state and the first and second law become

$$0 = \dot{W} + \sum_{\nu} \dot{Q}^{(\nu)}, \quad (28)$$

$$\dot{S}_i = - \sum_{\nu} \beta_{\nu} \dot{Q}^{(\nu)} \geq 0. \quad (29)$$

To indicate that we are at steady state, we dropped the time dependence on all quantities and for simplicity we will exclusively focus on the steady state regime for the rest of this paper. We also note that even for an undriven system there might be still a work source present (i.e., $\dot{W} \neq 0$) by identifying a work reservoir appropriately,

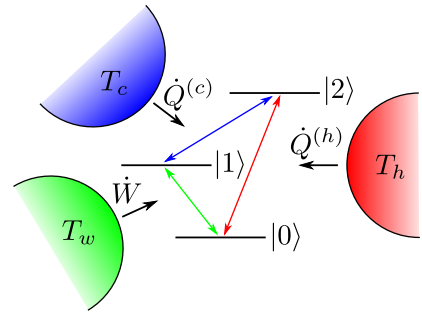


FIG. 3: (color online). Sketch of the maser heat engine where the working medium comprises three discrete levels and each transition is coupled to a separate reservoir called the hot (“h”, red), cold (“c”, blue) and work (“w”, green) reservoir. The black arrows indicate the direction in which we define energy flows to be positive.

see Sec. IV, or due to the possibility of particle transport (“chemical work”), see Sec. V.

Before we proceed to illustrate our theory with examples of heat engines working out of equilibrium, it might be worth to stress a simple consequence of our treatment at equilibrium. If the supersystem is time independent and in contact with only one reservoir at inverse temperature β , it will relax to an equilibrium state $\rho(t \rightarrow \infty) \sim e^{-\beta H'_S}$ such that the equilibrium state of the original system is [40]

$$\rho_S(t \rightarrow \infty) \sim \text{tr}_{\text{RC}} \{ e^{-\beta H'_S} \}. \quad (30)$$

This state in general does *not* equal the canonical equilibrium state of the system alone, i.e., $\rho_S(t \rightarrow \infty) \not\sim e^{-\beta H_S}$. Experimentally, deviations from the canonical state $e^{-\beta H_S}$ might be a clear indicator for persistent system environment correlations making it necessary to go beyond the Born approximation, e.g., by using the RC mapping. Given the SD of the reservoir, it should be then possible to test the prediction (30) in an actual experiment.

IV. APPLICATION I: THREE-LEVEL-MASER HEAT ENGINE

A. Standard treatment without RC

Possibly the simplest heat engine one can think of consists of three time-independent levels described by the Hamiltonian

$$H_S = \sum_{i=0}^2 \epsilon_i |i\rangle \langle i| \quad (31)$$

with $\epsilon_0 < \epsilon_1 < \epsilon_2$. The idea behind this engine is the model of a simple maser which is lasing at a particular transition, say $0 \leftrightarrow 1$. This lasing corresponds to “work”

⁵ In presence of particle transport the heat flow $\dot{Q}^{(\nu)}(t) = I_E^{(\nu)}(t) - \mu_{\nu} I_M^{(\nu)}(t)$ is composed of an energy current $I_E^{(\nu)}(t) = \text{tr}\{H'_S(t) \mathcal{L}^{(\nu)}(t) \rho(t)\}$ and a matter current $I_M^{(\nu)}(t) = \text{tr}\{N'_S \mathcal{L}^{(\nu)}(t) \rho(t)\}$ flowing into the supersystem. The first law then predicts energy conservation, $\frac{d}{dt} E(t) = \dot{W}(t) + \sum_{\nu} I_E^{(\nu)}(t)$, and particle number conservation, $\frac{d}{dt} N(t) = \sum_{\nu} I_M^{(\nu)}(t)$.

output and it is achieved due to population inversion between the levels $|0\rangle$ and $|1\rangle$. This in turn can be mediated via a third level $|2\rangle$ due to the presence of two heat reservoirs at different temperatures (called the “hot” and “cold” reservoir respectively), also see Fig. 3 for a sketch. Initially, this model was investigated in 1959 [55], but it is still of interest today [56–60].

The coupling to the reservoirs is mediated by the system operators

$$s_h = \frac{|0\rangle\langle 2| + |2\rangle\langle 0|}{\sqrt{2}\epsilon}, \quad (32)$$

$$s_c = \frac{|1\rangle\langle 2| + |2\rangle\langle 1|}{\sqrt{2}\epsilon}, \quad (33)$$

$$s_w = \frac{|0\rangle\langle 1| + |1\rangle\langle 0|}{\sqrt{2}\epsilon}. \quad (34)$$

Here, in units where $\hbar = 1$, the parameter ϵ has units of an energy or frequency such that s_ν has the same units as the coordinates $x_{k,\nu}$ of the bath oscillators. However, in all numerical calculations which follow we will simply set $\epsilon \equiv 1$. Within the standard approach (BMS approximation for the system only) the thermal generators $\mathcal{L}^{(\nu)}$ in Eq. (19) of each bath become

$$\mathcal{L}^{(h)} = \frac{J_0^{(h)}(\Delta_{20})}{\epsilon} \{[1 + n_h(\Delta_{20})]\mathcal{D}_{02} + n_h(\Delta_{20})\mathcal{D}_{20}\},$$

$$\mathcal{L}^{(c)} = \frac{J_0^{(c)}(\Delta_{21})}{\epsilon} \{[1 + n_c(\Delta_{21})]\mathcal{D}_{12} + n_c(\Delta_{21})\mathcal{D}_{21}\},$$

$$\mathcal{L}^{(w)} = \frac{J_0^{(w)}(\Delta_{10})}{\epsilon} \{[1 + n_w(\Delta_{10})]\mathcal{D}_{01} + n_w(\Delta_{10})\mathcal{D}_{10}\}.$$

Here, we have introduced the dissipator $\mathcal{D}_{ij}\rho \equiv |i\rangle\langle j|\rho|j\rangle\langle i| - \frac{1}{2}\{|j\rangle\langle j|\rho\}$, the Bose distribution $n_\nu(\Delta_{ij}) \equiv (e^{\beta_\nu\Delta_{ij}} - 1)^{-1}$ and the SDs $J_0^{(\nu)}(\omega)$ of bath ν are evaluated at the transition frequency $\Delta_{ij} \equiv \epsilon_i - \epsilon_j$.

Given the prescription of Sec. III, it is not hard to compute the thermodynamic behaviour of our system. At steady state the first law becomes $0 = \dot{W} + \dot{Q}^h + \dot{Q}^c$ with $\dot{W} \equiv \dot{Q}^w$ while the second law states that $-\beta_w\dot{W} - \beta_h\dot{Q}^h - \beta_c\dot{Q}^c \geq 0$. To quantify the performance of work extraction (i.e., $\dot{W} < 0$), we introduce the efficiency of the heat engine:

$$\eta \equiv \frac{-\dot{W}}{\dot{Q}^h} = \frac{\Delta_{10}}{\Delta_{20}} \leq \frac{\beta_c - \beta_h}{\beta_c - \beta_w} \quad (35)$$

where the inequality is a consequence of the second law. Furthermore and very remarkably, it is possible to show that the efficiency of the maser heat engine is always given by the ratio Δ_{10}/Δ_{20} independent of all other parameters (as long as $\dot{W} < 0$, of course).

Note that to completely justify the notion of a “work reservoir”, we should take the limit $\beta_w \rightarrow 0$ [59, 60], which complies with Sommerfelds notion of temperature as the “work value of heat” [61]. In this limit the entropy

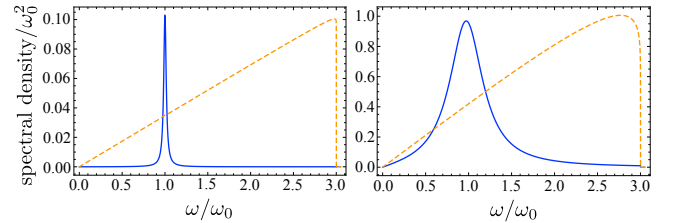


FIG. 4: (color online). Plot of the SDs $J_0^{(c)}(\omega)$ [Eq. (37), blue, solid] and $J_1^{(c)}(\omega)$ [determined by Eq. (12), orange, dashed] over ω/ω_0 for two different values of γ and d_0 : $\gamma = 0.035\omega_0, d_0 = 0.06\omega_0$ (left) and $\gamma = 0.47\omega_0, d_0 = 0.67\omega_0$ (right) and $\omega_R = 3\omega_0$ in both cases. We recognize a pronounced peak at $\omega \approx \omega_0$ for small γ in $J_0^{(c)}(\omega)$ whereas the shape of $J_1^{(c)}(\omega)$ remains rather unaffected.

change $-\beta_w\dot{W}$ in the work reservoir w goes to zero, the second law acquires the form $-\beta_h\dot{Q}^h - \beta_c\dot{Q}^c \geq 0$ and the efficiency (35) is bounded by Carnot efficiency $\eta_{\text{Carnot}} = 1 - \frac{T_c}{T_h}$. Microscopically, however, we recognize that the Bose distribution $n_w(\Delta_{10})$ diverges for $\beta_w \rightarrow 0$ (though \dot{W} remains finite), unless we additionally require that the bath SD scales like $J_0^{(w)}(\Delta_{10}) = \beta_w\Delta_{10}\Gamma_w$ for small β_w . In this ideal limit we then obtain

$$\lim_{\beta_w \rightarrow 0} \mathcal{L}^{(w)} = \Gamma_w(\mathcal{D}_{01} + \mathcal{D}_{10}), \quad (36)$$

i.e., the rates of upward and downward transitions are equal. However, for all numerical results reported below we take β_w to be small but non-zero.

Now, our approach is to consider the situation where it is actually not valid to apply this BMS ME for the system only. For instance, this could be due to a structured (non-Markovian) SD. In this case, one should actually use a non-Markovian ME for the system (e.g., the Redfield equation [52]). However, the thermodynamic interpretation of non-Markovian MEs is not clear and has not been established yet. In contrast, within our approach we know that we can include a RC into our description in order to account for non-Markovian effects on the three-level system (3LS) while the 3LS and RC evolve in a Markovian way. Any deviations from the efficiency Δ_{10}/Δ_{20} then indicate non-Markovian and/or strong coupling effects which we would be unable to detect by using the naive ME approach outlined in this section.

B. Thermodynamics with RC

For definiteness we choose the SD of the cold bath to be parameterized as

$$J_0^{(c)}(\omega) = \frac{d_0^2\gamma\omega}{(\omega^2 - \omega_0^2)^2 + \gamma^2\omega^2} \Theta(\omega_R - \omega), \quad (37)$$

while we still assume that it is safe to apply the Markov approximation with respect to the interaction with the

hot and work reservoir. Thus, by following the prescription of Sec. II we obtain the modified system Hamiltonian

$$H'_S = \sum_{i=0}^2 \epsilon_i |i\rangle\langle i| + \frac{1}{2} \left[P_1^2 + \frac{\lambda_0^2}{\delta\Omega_0^2} \left(X_1 - \frac{\delta\Omega_0^2}{\lambda_0} s_c \right)^2 \right], \quad (38)$$

and the SD $J_1^{(c)}(\omega)$ of the residual cold bath is determined by Eq. (12). In Fig. 4 we plot $J_0^{(c)}(\omega)$ and $J_1^{(c)}(\omega)$ for comparison.

At this point it is noteworthy that similar models have been also used in quantum biology to model light-harvesting complexes [62, 63]. Indeed, guided by this motivation, a number of researchers have started to investigate light-harvesting complexes from a heat engine perspective [64, 65] though we wish to stress that the models used there are not exactly the same as the one used here. Furthermore, Ref. [64] models the work reservoir effectively as a zero temperature reservoir, which causes divergences in the standard thermodynamic formalism. In Ref. [65] the polaron transformation was used in order to access strong coupling effects. We will introduce this transformation in Sec. V for a different model to compare it with our RC method.

To proceed we first of all note that the system Hamiltonian can be alternatively written as

$$H'_S = \left(\Delta_{10} + \frac{\delta\Omega_0^2}{4\epsilon} \right) |1\rangle\langle 1| + \left(\Delta_{20} + \frac{\delta\Omega_0^2}{4\epsilon} \right) |2\rangle\langle 2| - \frac{\lambda_0}{\sqrt{2}\epsilon} X_1 (|1\rangle\langle 2| + |2\rangle\langle 1|) + \frac{1}{2} \left(P_1^2 + \frac{\lambda_0^2}{\delta\Omega_0^2} X_1^2 \right), \quad (39)$$

where we made use of the fact that we can choose the ground state energy of the 3LS arbitrarily and set it to $\epsilon_0 \equiv 0$. This Hamiltonian describes a Rabi model (harmonic oscillator coupled to a two-level system) plus one additional energy level $|0\rangle$. Especially note that the energy levels of state $|1\rangle$ and $|2\rangle$ get both shifted by the same amount $\delta\Omega_0^2/4\epsilon$. In the weak coupling (but non-Markovian) regime – in which we wish to compare our extended model with the one treated before – these terms become negligible small.

To investigate the thermodynamic behaviour of our system, we will now use a ME which is explicit concerning the system-RC interaction, but treats the coupling to the other reservoirs perturbatively and in a Markovian way. Following standard procedures [6, 8, 9, 52] it is then possible to derive the BMS ME of the form (19) with time-independent Hamiltonian H'_S and dissipators $\mathcal{L}^{(\nu)}$. Thus, the thermodynamic treatment follows straightforwardly from Sec. III and is formally equivalent to the model of Sec. IV A. Hence, the first and second law become at steady state

$$0 = \dot{Q}^h + \dot{Q}^c + \dot{W}, \quad (40)$$

$$0 \leq -\beta_h \dot{Q}^h - \beta_c \dot{Q}^c - \beta_w \dot{W}. \quad (41)$$

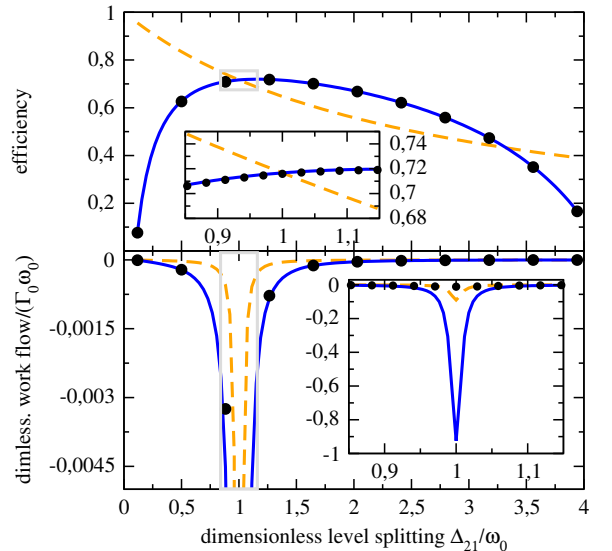


FIG. 5: (color online). Comparison of the efficiency (top) and the dimensionless work flow $\dot{W}/(\Gamma_h\omega_0)$ (bottom) of the non-Markovian heat engine including the RC (BMS ME: blue solid lines; ME without secular approximation: black dots) and the corresponding Markovian theory without RC from Sec. IV A (orange dashed lines) as a function of the level splitting Δ_{21}/ω_0 . The insets zoom into the region indicated by the grey box in the main figures. Parameters of the SD (37) are $d_0 = 0.0104\omega_0^2$, $\gamma = 0.0176\omega_0$, $\omega_R = 588\omega_0$, and $\omega_0 = 0.17$. Furthermore, we chose $\Delta_{10} = 2.53\omega_0$, $\beta_w\omega_0 = 0.0017$, $\beta_h\omega_0 = 0.17$ and $\beta_c\omega_0 = 17$ (implying a Carnot efficiency of $\eta_{\text{Carnot}} = 0.99$). Finally, to completely specify the model we also need to fix the SDs of the hot and work reservoir, which are determined by the coupling rates $\Gamma_w = 20\Gamma_h$ and $\Gamma_h = 0.001$, see Appendix B.

Now, however, we used a tilde on all energy flows because they are numerically different from the corresponding quantities in Sec. IV A. Likewise we introduce the efficiency of our engine for $\dot{W} < 0$ as

$$\tilde{\eta} = \frac{-\dot{W}}{\dot{Q}^h}, \quad (42)$$

which is also bounded by the Carnot efficiency in the limit $\beta_w \rightarrow 0$.

Because it is not possible to diagonalize the Hamiltonian (39) in a simple manner, one has to treat the ME numerically, and technical details of the derivation are presented in the Appendix B. We also note that we decided to compare the ME based only on the Born and Markov approximation (i.e., *without* secular approximation) with the BMS ME. The latter is usually only well justified for systems where the level spacing is much larger than the level broadening. This becomes increasingly questionable for more complex systems with many different (and not always well separated) eigen frequencies. On the other hand, the advantage of the BMS ME is that the resulting generator is of Lindblad form and allows for a mathematically clear proof of Spohn's inequality (27) [3, 8, 52]. In

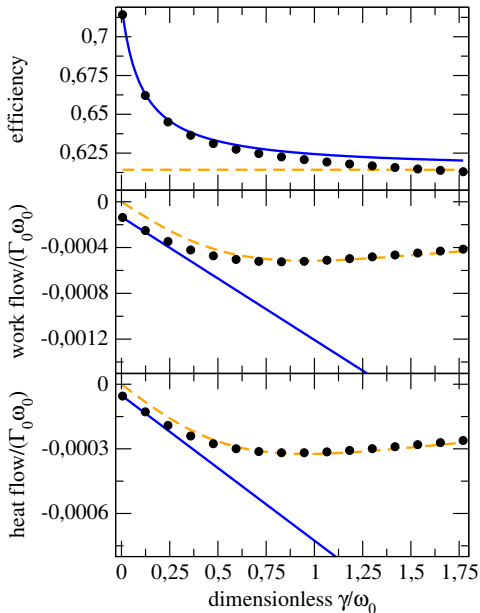


FIG. 6: (color online). Comparison of the efficiency, the dimensionless work flow $\dot{W}/(\Gamma_h \omega_0)$ and the dimensionless heat flow $\dot{Q}^{(c)}/(\Gamma_h \omega_0)$ into the cold reservoir of the non-Markovian heat engine including the RC (BMS ME: blue solid lines; ME without secular approximation: black dots) and the corresponding Markovian theory without RC from Sec. IV A (orange dashed lines) as a function of γ [see Eq. (37)]. All parameters are as in Fig. 5 except that $\Delta_{20} = 4.12\omega_0$.

the numerical results reported below, however, we never found any violation of the second law even when we used the ME without secular approximation.

Figs. 5, 6 and 7 show numerical results obtained from the model without RC (dashed lines, see Sec. IV A) and with RC [with (solid lines) and without (dots) secular approximation] for a specific choice of parameters. This choice was done to illustrate – from our point of view – interesting features of Markovian and non-Markovian heat engines. However, a detailed investigation of the model is beyond the scope of the paper and would also be questionable because the model from Sec. IV A clearly is a simplified toy model. Nevertheless, we wish to remark that the qualitative behaviour of our numerical results remains the same for a wide range of parameters. Furthermore, we have focused on plots of the efficiency and work, which are both of great interest in thermodynamics: obviously, we want to have a large power output, but on the other hand, a large power output does not mean that our engine works more efficiently. In fact, if we possess a heat engine with low power output but high efficiency, we can also build a machine with high power output and the same efficiency by running several of these machines in parallel. Hence, we think efficiency is a more universal quantity on which one should put more emphasis in the study of heat engines in the strong coupling and non-Markovian regime.

Turning to the details, we can infer from Fig. 5 two

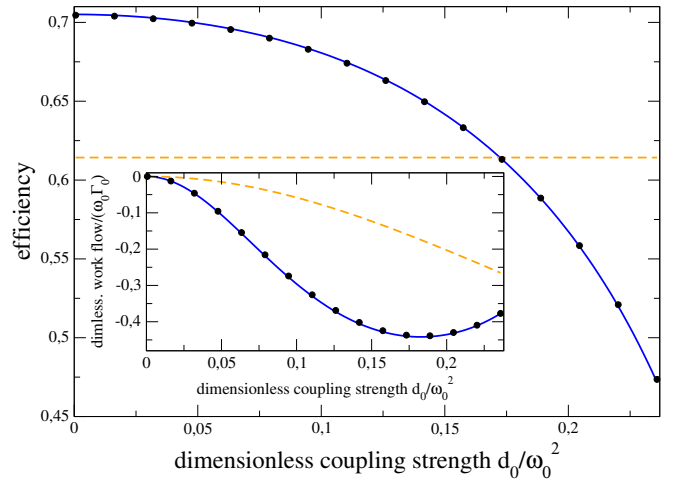


FIG. 7: (color online). Comparison of the efficiency and the dimensionless work flow $\dot{W}/(\Gamma_h \omega_0)$ (inset) of the non-Markovian heat engine including the RC (BMS ME: blue solid lines; ME without secular approximation: black dots) and the corresponding Markovian theory without RC from Sec. IV A (orange dashed lines) as a function of the system-RC coupling strength d_0/ω_0^2 . All parameters are as in Fig. 5 except that $\Delta_{20} = 4.12\omega_0$.

important points. First, our approach predicts an efficiency enhancement of 10% to 20% in comparison to the standard theoretical framework from Sec. IV A. We here note that it makes sense to compare the model without and with RC because all parameters of the latter are completely fixed by the initial model. We simply use two different theoretical methods to study the *same* engine, but only the latter allows to capture, e.g., non-Markovian effects. The second point to note concerns the secular approximation. Whereas for a large parameter regime it seems to be remarkably well justified, it can also completely fail by predicting a nearly hundred times larger power output for the case $\Delta_{21} \approx \omega_0$ (interestingly, this effect cancels when we compute the efficiency). In fact, if this resonance condition is met⁶, many energy levels are very close to each other (though never exactly degenerate) and a naive application of the secular approximation is not justified.

In Fig. 6 we show the efficiency, work and heat flow as a function of γ . As we can infer from Eq. (37) (also see Fig. 4) a smaller γ implies a stronger peaked SD $J_0^{(c)}(\omega)$. Thus, γ can be seen as a measure of the non-Markovianity of the SD and Fig. 6 proves that this is the cause of the efficiency enhancement. This justifies our claim that non-Markovian machines can significantly outperform their

⁶ Note that ω_0 equals the frequency of the RC for large cutoff frequency ω_R , see appendix B.

Markovian counterparts *even at steady state*.⁷ Furthermore, Fig. 6 also shows that we recover the results from Sec. IV A in the limit of large γ . In fact, for large γ the SD does not only become more Markovian, but also the SD $J_1^{(c)}(\omega)$ of the residual cold bath is directly proportional to γ , see Eq. (B15), such that the RC evolves on time-scales much shorter than the 3LS and can be adiabatically eliminated. Furthermore, Fig. 6 also shows that the BMS ME of the supersystem completely fails in this regime. This behaviour can be traced back to the fact that the secular approximation does not commute with the adiabatic elimination of the RC, i.e., the time-scales involved in the coherent evolution of the system are of the same order as the dynamics of the relaxation due to the residual cold bath.

Finally, Fig. 7 shows the thermodynamics as a function of the system-RC coupling strength d_0 (or the coupling strength between the 3LS and the cold reservoir, respectively). Again, we can observe a strong efficiency enhancement and an almost perfect agreement between the secular and non-secular ME. Furthermore, we observe that the efficiency decreases as a function of d_0 while the power output first increases up to a certain critical coupling strength and then starts to decrease again (note that the power output for the 3LS ME from Sec. IV A reaches a constant value for $d_0 \rightarrow \infty$ instead). In fact, for all parameters we have checked we always observed a decreasing efficiency as a function of d_0 . Whether this is a general feature or model specific remains an open question, which might be eventually answerable within the RC framework.

V. APPLICATION II: SINGLE ELECTRON TRANSISTOR COUPLED TO VIBRATIONS

A. Model and RC mapping

As a second application we consider a single quantum dot in contact with two fermionic reservoirs (typically called a single electron transistor) and additionally coupled to a bath of phonons. Related models have been studied, e.g., in Refs. [31, 32, 66–69], in order to understand electronic transport through molecules where the phonon bath models molecular vibrations. Here, as well as outlining another model applicable to the RC method, we also wish to compare with the polaron transformation, a technique frequently used to access the regime of strong system-phonon coupling [29, 31–34, 68, 69]. We will discuss what we mean by that in more detail at the end of

Sec. V B.

The global Hamiltonian can be written as

$$H = H_{\text{dot}} + H_{\text{el}} + H_{\text{el-dot}} + H_{\text{ph}}. \quad (43)$$

The electronic part of the system is described by

$$H_{\text{dot}} = \epsilon d^\dagger d, \quad (44)$$

$$H_{\text{el}} = \sum_{\nu} \sum_k \epsilon_{k\nu} c_{k\nu}^\dagger c_{k\nu}, \quad (45)$$

$$H_{\text{el-dot}} = \sum_{\nu} \sum_k (t_{k\nu} c_{k\nu} d^\dagger + t_{k\nu}^* d c_{k\nu}^\dagger) \quad (46)$$

where $d^{(\dagger)}$ and $c_{k,\nu}^{(\dagger)}$ are fermionic annihilation (creation) operators of the dot and the reservoir with associated on-site energy ϵ and lead energy $\epsilon_{k\nu}$. Furthermore, the dot is connected to two leads $\nu \in \{L, R\}$ with tunneling amplitudes $t_{k\nu}$. The interaction of the dot with the phonon bath is assumed to be

$$H_{\text{ph}} = \frac{1}{2} \sum_q \left[p_q^2 + \omega_q^2 \left(x_q - \frac{h_q}{\omega_q^2} d^\dagger d \right)^2 \right]. \quad (47)$$

Here, we denoted the coupling coefficients to the phonon bath by h_q because we already use $c_{k\nu}$ for the electrons in the fermionic reservoirs.

Next, again in order to overcome the limitations of the usual BMS ME we employ the RC mapping, this time to the phonon bath. This transforms the system and phonon part to [see Eq. (7)]

$$\begin{aligned} H_{\text{dot}} + H_{\text{ph}} = & \quad (48) \\ & \left(\epsilon + \frac{1}{2} \sum_q \frac{h_q^2}{\omega_q^2} \right) d^\dagger d - \lambda_0 d^\dagger d X_1 + \frac{1}{2} (P_1^2 + \Omega_1^2 X_1^2) \\ & - X_1 \sum_q C_q X_q + \frac{1}{2} \sum_q (P_q^2 + \Omega_q^2 X_q^2). \end{aligned}$$

We now identify our supersystem to be

$$H'_S = \tilde{\epsilon} d^\dagger d - \lambda_0 d^\dagger d X_1 + \frac{1}{2} (P_1^2 + \Omega_1^2 X_1^2) \quad (49)$$

with $\tilde{\epsilon} \equiv \epsilon + \frac{1}{2} \sum_q h_q^2 / \omega_q^2$ whereas the interaction with the phonon bath is described via $H_I^{\text{ph}} = -X_1 \sum_q C_q X_q$ and the residual phonon bath Hamiltonian becomes $H_B^{\text{ph}} = \frac{1}{2} \sum_q (P_q^2 + \Omega_q^2 X_q^2)$. Note that this does not exactly correspond to the mapping (17), but now the Hamiltonian is closer to the literature to which we wish to compare our results [31]. Furthermore, the spectrum of H'_S is still bounded from below for all coupling strengths λ_0 .

Below it will be convenient to work with the bosonic ladder operators, which are related to position and momentum operators via

$$X_q = \frac{1}{\sqrt{2\Omega_q}} (a_q + a_q^\dagger), \quad P_q = i\sqrt{\frac{\Omega_q}{2}} (a_q - a_q^\dagger). \quad (50)$$

⁷ Note that Ref. [35] also demonstrates an increased ability to extract work due to non-Markovian effects. However, Ref. [35] did not study the efficiency and focused on transient effects, making it unclear whether a steadily working heat engine can be better than its Markovian counterpart.

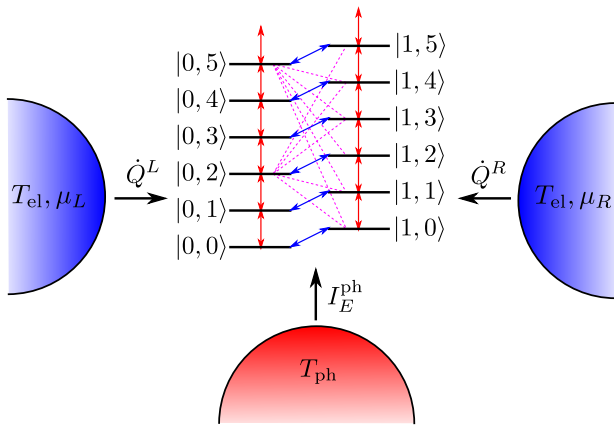


FIG. 8: (color online). This sketch shows the level structure of the Hamiltonian (55) with eigenstates $|n, m\rangle$. The phonon bath (red, vertical arrows) can induce transitions between states $|n, m\rangle \leftrightarrow |n, m+1\rangle$ whereas the electronic leads (blue, diagonal arrows) always change the occupation number n of the quantum dot. Furthermore, the jump of an electron in or out of the system can be also accompanied by multi-phonon transitions as exemplarily indicated with thin, dashed, magenta lines.

In terms of these operators we have

$$\tilde{H}_S = \tilde{\epsilon} d^\dagger d + \Omega_1 \left(a_1^\dagger a_1 + \frac{1}{2} \right) - \frac{\lambda_0 d^\dagger d}{\sqrt{2\Omega_1}} (a_1 + a_1^\dagger), \quad (51)$$

$$H_I^{\text{ph}} = - (a_1 + a_1^\dagger) \sum_q \frac{C_q}{2\sqrt{\Omega_1 \Omega_q}} (a_q + a_q^\dagger), \quad (52)$$

$$H_B^{\text{ph}} = \sum_q \Omega_q \left(a_q^\dagger a_q + \frac{1}{2} \right). \quad (53)$$

B. ME description

To deduce the BMS ME we need to diagonalize the system Hamiltonian (51). This can be accomplished via the unitary transformation (we introduce $\lambda \equiv \lambda_0/\sqrt{2\Omega_1}$ for brevity)

$$U = \exp \left[\frac{\lambda}{\Omega_1} d^\dagger d (a_1 - a_1^\dagger) \right]. \quad (54)$$

It transforms operators according to $U a_1 U^\dagger = a_1 + \frac{\lambda}{\Omega_1} d^\dagger d$ and $U d U^\dagger = d e^{-\frac{\lambda}{\Omega_1} (a_1 - a_1^\dagger)}$. Hence, applying (54) to H'_S yields

$$U H'_S U^\dagger = \bar{\epsilon} d^\dagger d + \Omega_1 \left(a_1^\dagger a_1 + \frac{1}{2} \right) \quad (55)$$

with $\bar{\epsilon} \equiv \tilde{\epsilon} - \lambda^2/\Omega_1$. This Hamiltonian is obviously in diagonal form with eigenstates $|n, m\rangle$, where $n \in \{0, 1\}$ ($m \in \{0, 1, 2, \dots\}$) quantifies the electronic (bosonic) occupation, and eigenenergies $E_{nm} = \bar{\epsilon} n + \Omega_1 (m + \frac{1}{2})$.

Given the spectral decomposition of the Hamiltonian it is simple to deduce the BMS ME, especially if the spectrum is non-degenerate, which will generically be the case (unless $\bar{\epsilon}$ coincides with Ω_1). To completely specify our model we choose to define and parametrize the SD of the fermionic leads as

$$\Gamma_\nu(\omega) \equiv 2\pi \sum_k |t_{k\nu}|^2 \delta(\omega - \epsilon_{k\nu}) = \frac{\Gamma_\nu \delta_\nu^2}{(\omega - \epsilon_\nu)^2 + \delta_\nu^2}. \quad (56)$$

Here, δ_ν quantifies the width and ϵ_ν the maximum of the Lorentzian function. Furthermore, the SD of the residual phonon bath is chosen to be ohmic with exponential cutoff,

$$J_1(\omega) = J_{\text{ph}} \omega e^{-|\omega|/\omega_R}, \quad (57)$$

which for large cutoff frequencies ω_R corresponds to an initial SD of the form (37) (as discussed at the end of Appendix B). Further technical details concerning the derivation of the BMS ME are provided in Appendix C. A sketch of the resulting dynamics is provided in Fig. 8.

Before we proceed to show numerical results, let us briefly explain an alternative way to treat strong system-phonon interaction and to which we refer as the polaron ME (PME). Similarly to the RC mapping, also the PME starts with a unitary transformation, which acts on the bath *and* system Hilbert space though. This transformation usually has the form of a generalized displacement operation such as (54). Then, within this displaced reference frame it is possible to treat the coupling as a small perturbation again because the strong part is absorbed in this new frame. Consequently, it is possible to derive a ME valid for strong coupling for the *system part only* (in our case here the quantum dot). In contrast, for our treatment we explicitly include the RC as a part of the (super) system and use the transformation (54) later on only to formally diagonalize the supersystem.

C. Results

In Fig. 9 we plot the matter current from left to right versus the difference in chemical potentials $V = \mu_L - \mu_R$ of the electronic reservoirs. First, we see that at low electronic temperatures, the current displays multiple steps, which occur at $V_i = 2\Delta E_i$, where ΔE_i are the transition frequencies of the system. Thus, the steps enable one to deduce the renormalized electron energy $\bar{\epsilon}$ and the phonon frequency Ω_1 from the electronic current. Furthermore, if we truncate the phonon Hilbert space at a small cutoff number N_c , we see that only few plateaus are visible since the number of possible transitions is bounded. Most notably, however, when both N_c is large enough and the coupling between the RC and the residual oscillators is large, we reproduce earlier results based on a PME [31] (solid curves). In fact, for a large coupling between the RC and its environment, the RC will thermalize on much shorter time-scales as compared to

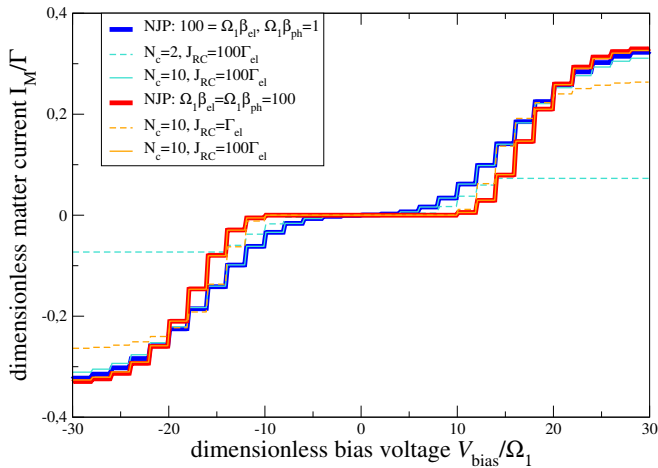


FIG. 9: (color online). Plot of matter current versus bias voltage for equal electronic tunneling rates $\Gamma_L = \Gamma_R = \Gamma$. Previous results (bold curves, taken from [31]) are reproduced when the coupling to the residual oscillators is much larger than to the electronic leads ($J_{\text{ph}} \gg \Gamma$) and when the cutoff N_c in the number of considered phonon modes is sufficiently large. Other parameters have been chosen as $\delta_L = \delta_R = 10\Omega_1$, $\varepsilon_L = \varepsilon_R = 0$, $\omega_R = 10\Omega_1$, $\tilde{\varepsilon} = 0$, $\lambda_0 = \sqrt{5}\Omega_1^{3/2}$.

the dot-lead evolution. This is exactly the regime of the PME in which it is assumed *ad hoc* that the environment in the polaron frame is equilibrated with respect to the dot state. We thus see that the RC method gives us a way to physically and mathematically justify the PME, but in general will be also applicable beyond that regime.

Finally, we want to turn to the question whether it is possible to use our setup as a thermoelectric device, i.e., whether we can pump electrons against the bias due to a temperature gradient between electronic leads and phonon reservoir. From Fig. 9 we see that we have zero current at zero bias even for different temperatures of the electronic and phononic reservoirs (blue and turquoise). This is due to the fact that we chose $\delta_L = \delta_R$ and $\varepsilon_L = \varepsilon_R$ [see Eq. (56)], which makes our setup symmetric under exchanging the labels L and R at zero bias. This makes thermoelectric transport impossible and will be changed now.

To quantify the irreversibility of our device we take a look at the entropy production (29),

$$\begin{aligned} \dot{S}_i &= -\beta_L \dot{Q}^L - \beta_R \dot{Q}^R - \beta_{\text{ph}} \dot{Q}^{\text{ph}} \\ &= \beta_{\text{el}}(\mu_L - \mu_R)I_M + (\beta_{\text{el}} - \beta_{\text{ph}})I_E \geq 0. \end{aligned} \quad (58)$$

For the last line we assumed equal temperatures in the electronic leads $\beta_L = \beta_R = \beta_{\text{el}}$ and we used matter conservation $I_M \equiv +I_M^L = -I_M^R$ and energy conservation $I_E \equiv I_E^{\text{ph}} = -(I_E^L + I_E^R)$.

When the electronic and phononic temperatures are different (e.g. $\beta_{\text{el}} > \beta_{\text{ph}}$), heat will flow between the electronic and phononic reservoirs, and the device can use a fraction of the heat to produce positive power

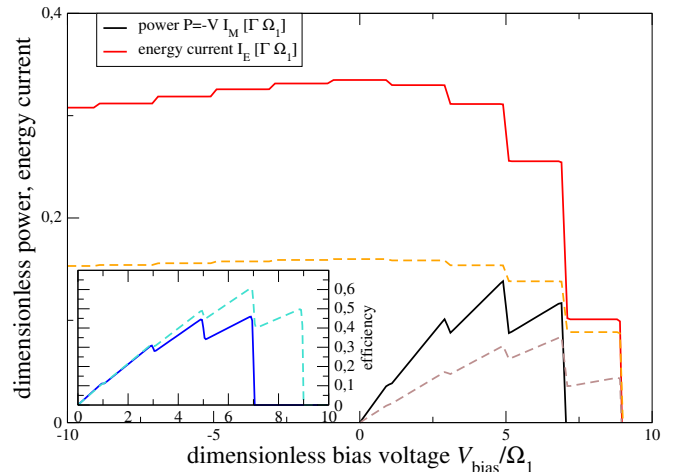


FIG. 10: (color online). Plot of dimensionless power (solid black, dashed gray) and dimensionless energy current (solid red, dashed orange) versus bias voltage for equal coupling strengths to all reservoirs $\Gamma_L = \Gamma_R = \Gamma = J_{\text{ph}}/2$. For $\delta_L = \delta_R = \Omega_1$ (solid curves) the efficiency (solid blue, inset) – defined only in the region of positive power – reaches about half Carnot efficiency at best. This is improved by narrowing the bandwidth to $\delta_L = \delta_R = 0.5\Omega_1$ (dashed curves). Other parameters have been chosen as $\varepsilon_L = +5\Omega_1 = -\varepsilon_R$, $\omega_R = 10\Omega_1$, $\tilde{\varepsilon} = 0$, $\lambda_0 = \Omega_1^{3/2}$, $\beta_{\text{el}}\Omega_1 = 100$, $\beta_{\text{ph}}\Omega_1 = 0.01$, $N_c = 10$.

$P = -(\mu_L - \mu_R)I_M$ by transporting charges against the bias. The positivity of the entropy production leads to an upper bound for the efficiency of heat-to-power conversion

$$\eta = \frac{-(\mu_L - \mu_R)I_M}{I_E}, \quad (59)$$

which is defined for $(\mu_L - \mu_R)I_M < 0$. As expected, one can show that the upper bound is given by Carnot efficiency.

To break the inherent left-right symmetry of our model, it is necessary to use different energy dependencies of the electronic tunneling rates. We therefore consider the limit $\delta_L = \delta_R = \delta$ but $\varepsilon_L \neq \varepsilon_R$. To make the effect rather strong we also have to consider δ smaller than $|\varepsilon_\nu|$, but the use of the system as a thermoelectric device does not require that $J_{\text{ph}} \gg \Gamma$. In Fig. 10 we plot the generated power and heat current from the hot phonon reservoir into the system versus the bias voltage. First, we see that there exists a region where the generated power becomes positive, meaning that charges are transported against the bias. This is only possible when heat flows from the phonon reservoir to the two electronic reservoirs, and within the region of positive power we can see that the efficiency (inset in Eq. (59)) becomes finite and reaches for our chosen parameters about half Carnot efficiency. We remark that a naive treatment of the quantum dot alone within a BMS ME would *always* predict $I_E = 0$ because $[H_{\text{dot}}, H_{\text{ph}}] = 0$ and thus, no transport

of electrons against the bias would be possible in this framework. Having non-zero energy transport $I_E \neq 0$ is indeed a higher order effect (i.e., beyond second order perturbation theory).

VI. FINAL REMARKS

We have presented a framework which allows to investigate thermal machines beyond the standard weak coupling and Markovian assumption. This treatment is general in the sense that it can be applied to any system where strong coupling effects and non-Markovianity are caused by a linear coupling with a bosonic bath. Our framework is by construction thermodynamically consistent because we simply apply the standard framework of quantum thermodynamics to an enlarged system. By this procedure we also automatically avoid spurious effects like efficiencies beyond Carnot. Thus, in a certain sense the RC mapping helps us to find the correct border for which it is allowed to partition the “universe” into a “system” and a “bath” part, i.e., the partition for which it is justified to apply the Born approximation.

Then, within this framework we have observed that non-Markovianity can indeed strongly enhance the efficiency of a heat engine even in the weak coupling limit. Furthermore, we also observed that strong coupling decreases the efficiency, though it is not clear at the moment whether this is a general feature. As another application we considered a single electron transistor coupled to vibrations, which is an important model to understand molecular transport. Besides studying its efficiency as a thermoelectric device we have demonstrated that the widely used PME follows from our treatment as a special case and hence, justifying the PME.

Though we believe that we have introduced a very useful and practical framework, one should also critically question it. Especially, there might be (at first sight) two weak points on which we would like to comment.

First, though it was shown in Refs. [44, 45] that the RC mapping is guaranteed to give a quasi-Ohmic (Markovian) SD after we have included a sufficient number of RCs, it is not guaranteed that the resulting final SD is also weak in the sense that it is justified to consider only second order perturbation theory in the coupling to the residual baths. Though we have seen in Sec. II that the overall coupling strength of the original system to the environment can be captured by using *only one* RC, the resulting final SD in general depends on the shape of the initial SD (but not on its “absolute value”) and might be

still large compared to parameters of the system. This has to be checked separately and if this turns out to be the case, one might need to perform an additional approximation or use other methods. Even if this is the case, however, the RC method still allows us to go beyond the standard perturbative approach in a reasonable way.

Second, one might object that the information about what happens to the original system itself is somehow lost. Indeed, it is true that we can only give expressions for the heat flows, the power and the entropy production for the supersystem, including the RCs, but we do not know them for any particular subsystem. However, we would defend this approach by the following remarks. First of all, the division of a thermodynamic system into subsystems (e.g., system and reservoirs) is in fact something which is only possible in the weak coupling limit. The very definition of “system” becomes ambiguous beyond that regime (also see the discussion on the zeroth law in [8]). Second, we point out that there has been progress to understand the energetics of arbitrary multipartite systems *locally* [70, 71] and for special situations this is also possible for the entropic balances [72, 73] (note that the meaning of “bipartite” in Refs. [72, 73] is more restrictive than in Refs. [70, 71]). This opens up a new interpretation of thermodynamics in the strong coupling and non-Markovian regime by recognizing the role played by the non-Markovian environment as an effective feedback controller who acts back on the system based on the information stored about it. Thus, advances in the thermodynamic understanding of multipartite systems will directly yield to new insights in the field of strong coupling and non-Markovian thermodynamics.

Acknowledgments

It is a pleasure to thank Javier Cerrillo, Mauro Cirio, Massimiliano Esposito, Jake Illes-Smith and Ahsan Nazir for valuable discussions. In addition, we explicitly wish to thank David Newman and Ahsan Nazir for sharing their related manuscript on thermodynamics and the reaction coordinate method prior to publication [38]. Furthermore, PS is especially indebted to Rocco Martinazzo for very helpful correspondence concerning the RC mapping. Financial support of the DFG (SCHA 1646/3-1, SFB 910, and GRK 1558) is gratefully acknowledged. NL is partially supported by the FY2015 Incentive Research Project.

-
- [1] J. C. Maxwell, *Theory of Heat* (Longmans, Greens, and Co., London, 1871).
 - [2] E. H. Lieb and J. Yngvason, *Phys. Rep.* **310**, 1 (1999).
 - [3] H. Spohn, *J. Math. Phys.* **19**, 1227 (1978).
 - [4] H. Spohn and J. L. Lebowitz, *Adv. Chem. Phys.* **38**, 109

- (1979).
- [5] R. Alicki, *J Phys. A* **12**, L103 (1979).
- [6] M. Esposito, U. Harbola, and S. Mukamel, *Rev. Mod. Phys.* **81**, 1665 (2009).
- [7] M. Campisi, P. Hänggi, and P. Talkner, *Rev. Mod. Phys.*

- 83**, 771 (2011).
- [8] R. Kosloff, Entropy **15**, 2100 (2013).
- [9] G. Schaller, *Open Quantum Systems Far from Equilibrium* (Lect. Notes Phys., Springer, Cham, 2014).
- [10] D. Gelbwaser-Klimovsky, W. Niedenzu, and G. Kurizki, Adv. At. Mol. Opt. Phys. **64**, 329 (2015).
- [11] T. Speck and U. Seifert, J. Stat. Mech. **L09002** (2007).
- [12] M. Esposito, K. Lindenberg, and C. Van den Broeck, New J. Phys. **12**, 013013 (2010).
- [13] J. Ankerhold and J. P. Pekola, Phys. Rev. B **90**, 075421 (2014).
- [14] C. Jarzynski, J. Stat. Mech. **P09005** (2004).
- [15] M. Campisi, P. Talkner, and P. Hänggi, Phys. Rev. Lett. **102**, 210401 (2009).
- [16] U. Seifert, Phys. Rev. Lett. **116**, 020601 (2016).
- [17] T. Kawamoto and N. Hatano, Phys. Rev. E **84**, 031116 (2011).
- [18] B. Leggio, A. Napoli, H. P. Breuer, and A. Messina, Phys. Rev. E **87**, 032113 (2013).
- [19] S. Vinjanampathy and K. Modi, arXiv: 1411.7755 (2014).
- [20] S. Vinjanampathy and K. Modi, Phys. Rev. A **92**, 052310 (2015).
- [21] M. Esposito, M. A. Ochoa, and M. Galperin, Phys. Rev. Lett. **114**, 080602 (2015).
- [22] G. E. Topp, T. Brandes, and G. Schaller, Europhys. Lett. **110**, 67003 (2015).
- [23] M. Esposito, M. A. Ochoa, and M. Galperin, Phys. Rev. B **92**, 235440 (2015).
- [24] A. Bruch, M. Thomas, S. V. Kusminskiy, F. von Oppen, and A. Nitzan, arXiv: 1511.03276 (2015).
- [25] R. Adamietz, G.-L. Ingold, and U. Weiss, Eur. Phys. J. B **87**, 90 (2014).
- [26] M. Carrega, P. Solinas, A. Braggio, M. Sasseti, and U. Weiss, New J. Phys. **17**, 045030 (2015).
- [27] T. G. Philbin and J. Anders, arXiv: 1512.02551 (2015).
- [28] D. Segal, Phys. Rev. B **73**, 205415 (2006).
- [29] L. Nicolin and D. Segal, Phys. Rev. B **84**, 161414(R) (2011).
- [30] K. Saito and T. Kato, Phys. Rev. Lett. **111**, 214301 (2013).
- [31] G. Schaller, T. Krause, T. Brandes, and M. Esposito, New J. Phys. **15**, 033032 (2013).
- [32] T. Krause, T. Brandes, M. Esposito, and G. Schaller, J. Chem. Phys. **142**, 134106 (2015).
- [33] C. Wang, J. Ren, and J. Cao, Sci. Rep. **5**, 11787 (2015).
- [34] D. Gelbwaser-Klimovsky and A. Aspuru-Guzik, J. Phys. Chem. Lett. **6**, 3477 (2015).
- [35] B. Bylicka, M. Tukiainen, J. Piilo, D. Chruscinski, and S. Maniscalco, arXiv: 1504.06533 (2015).
- [36] R. Gallego, A. Riera, and J. Eisert, New J. Phys. **16**, 125009 (2014).
- [37] A. Garg, J. N. Onuchic, and V. Ambegaokar, J. Chem. Phys. **83**, 4491 (1985).
- [38] D. Newman, F. Mintert, and A. Nazir, In preparation .
- [39] R. Martinazzo, K. H. Hughes, and I. Burghardt, Phys. Rev. E **84**, 030102 (2011).
- [40] J. Iles-Smith, N. Lambert, and A. Nazir, Phys. Rev. A **90**, 032114 (2014).
- [41] M. Bonfanti, K. H. Hughes, I. Burghardt, and R. Martinazzo, Ann. Phys. **00**, 1 (2015).
- [42] J. Iles-Smith, A. G. Dijkstra, N. Lambert, and A. Nazir, arXiv: 1511.05181 (2015).
- [43] A. W. Chin, A. Rivas, S. F. Huelga, and M. B. Plenio, J. Math. Phys. **51**, 092109 (2010).
- [44] R. Martinazzo, B. Vacchini, K. H. Hughes, and I. Burghardt, J. Chem. Phys. **134**, 011101 (2011).
- [45] M. P. Woods, R. Groux, A. W. Chin, S. F. Huelga, and M. B. Plenio, J. Math. Phys. **55**, 032101 (2014).
- [46] U. Weiss, *Quantum Dissipative Systems* (World Scientific, 3rd ed, Singapore, 2008).
- [47] C. Gardiner and P. Zoller, *Quantum Noise* (Springer-Verlag, Berlin Heidelberg, 2004).
- [48] G. W. Ford, J. T. Lewis, and R. F. O'Connell, Phys. Rev. A **37**, 4419 (1988).
- [49] M. M. Wolf, J. Eisert, T. S. Cubitt, and J. I. Cirac, Phys. Rev. Lett. **101**, 150402 (2008).
- [50] H. P. Breuer, E.-M. Laine, and J. Piilo, Phys. Rev. Lett. **103**, 210401 (2009).
- [51] A. Rivas, S. F. Huelga, and M. B. Plenio, Phys. Rev. Lett. **103**, 050403 (2010).
- [52] H. P. Breuer and F. Petruccione, *The Theory of Open Quantum Systems* (Oxford University Press, Oxford, 2002).
- [53] G. Bulnes Cuetara, A. Engel, and M. Esposito, New J. Phys. **17**, 055002 (2015).
- [54] S. Deffner and E. Lutz, Phys. Rev. Lett. **107**, 140404 (2011).
- [55] H. E. D. Scovil and E. O. Schulz-DuBois, Phys. Rev. Lett. **2**, 262 (1959).
- [56] E. Geva and R. Kosloff, J. Chem. Phys. **104**, 7681 (1996).
- [57] E. Boukobza and D. J. Tannor, Phys. Rev. Lett. **98**, 240601 (2007).
- [58] L. A. Correa, J. P. Palao, D. Alonso, and G. Adesso, Sci. Rep. **4**, 3949 (2014).
- [59] R. Kosloff and A. Levy, Annu. Rev. Phys. Chem. **65**, 365 (2014).
- [60] L. A. Correa, J. P. Palao, G. Adesso, and D. Alonso, Phys. Rev. E **90**, 062124 (2014).
- [61] A. Sommerfeld, *Atomic Structure and Spectral Lines* (Methuen & Co Ltd, London, 1923).
- [62] N. Lambert, Y. N. Chen, Y. C. Cheng, C. M. Li, G. Y. Chen, and F. Nori, Nat. Phys. **9**, 10 (2013).
- [63] S. F. Huelga and M. B. Plenio, Contemp. Phys. **54**, 181 (2013).
- [64] N. Killoran, S. F. Huelga, and M. B. Plenio, J. Chem. Phys. **143**, 155102 (2015).
- [65] D. Xu, C. Wang, Y. Zhao, and J. Cao, arXiv: 1508.04708 (2015).
- [66] J. Koch and F. von Oppen, Phys. Rev. Lett. **94**, 206804 (2005).
- [67] O. Entin-Wohlman, Y. Imry, and A. Aharony, Phys. Rev. B **82**, 115314 (2010).
- [68] S. Maier, T. L. Schmidt, and A. Komnik, Phys. Rev. B **83**, 085401 (2011).
- [69] A. J. White and M. Galperin, Phys. Chem. Chem. Phys. **14**, 13809 (2012).
- [70] H. Weimer, M. J. Henrich, F. Rempp, H. Schröder, and G. Mahler, Europhys. Lett. **83**, 30008 (2008).
- [71] H. Hossein-Nejad, E. J. O'Reilly, and A. Olaya-Castro, New J. Phys. **17**, 075014 (2015).
- [72] D. Hartich, A. C. Barato, and U. Seifert, J. Stat. Mech. **P02016** (2014).
- [73] J. M. Horowitz and M. Esposito, Phys. Rev. X **4**, 031015 (2014).
- [74] A. J. Leggett, Phys. Rev. B **30**, 1208 (1984).
- [75] G. Schaller and T. Brandes, Phys. Rev. A **78**, 022106 (2008).

Appendix A: Mapping of the spectral densities

We will here prove Eq. (12) following the way of Martinazzo *et al.* [44]; for other derivations see Refs. [37, 40, 43, 45]. Because the system is completely arbitrary in our treatment, we will choose for the moment without loss of generality a particle with position q and momentum p moving in a potential $V(q)$. The equations of motion according to the original Hamiltonian (2) then take on the form

$$\ddot{q} = -\frac{\partial V}{\partial q} + \sum_k c_k x_k - \sum_k \frac{c_k^2}{\omega_k^2} q, \quad (\text{A1})$$

$$\ddot{x}_k = -\omega_k^2 x_k + c_k q. \quad (\text{A2})$$

After Fourier transformation according to the definition

$$\hat{f}(z) \equiv \int_{-\infty}^{\infty} dt e^{izt} f(t) \quad (\Im(z) > 0), \quad (\text{A3})$$

we obtain

$$-z^2 \hat{q} = -\frac{\partial \widehat{V}}{\partial q} + \sum_k c_k \hat{x}_k - \sum_k \frac{c_k^2}{\omega_k^2} \hat{q}, \quad (\text{A4})$$

$$-z^2 \hat{x}_k = -\omega_k^2 \hat{x}_k + c_k \hat{q}. \quad (\text{A5})$$

Eliminating \hat{x}_k we can write

$$-\frac{\partial \widehat{V}}{\partial q} = \hat{L}_0(z) \hat{q}. \quad (\text{A6})$$

with the Fourier space propagator

$$\begin{aligned} \hat{L}_0(z) &= -z^2 - \sum_k \frac{c_k^2}{\omega_k^2 - z^2} + \sum_k \frac{c_k^2}{\omega_k^2}, \\ &\equiv -z^2 - W_0(z) + \delta\Omega_0^2. \end{aligned} \quad (\text{A7})$$

Here, we have introduced the Cauchy transform of $J_0(\omega)$:

$$W_0(z) \equiv \frac{2}{\pi} \int_0^{\infty} d\omega \frac{\omega J_0(\omega)}{\omega^2 - z^2} = \frac{1}{\pi} \int_{-\infty}^{\infty} d\omega \frac{J_0(\omega)}{\omega - z} \quad (\text{A8})$$

where we used $J_0(-\omega) = -J_0(\omega)$. As Leggett noticed [74], the SD of the bath is linked to the propagator via

$$J_0(\omega) = -\lim_{\epsilon \searrow 0} \Im[\hat{L}_0(\omega + i\epsilon)] \equiv -\Im[\hat{L}_0^+(\omega)] \quad (\omega \in \mathbb{R}). \quad (\text{A9})$$

Especially within our notation we have $J_0(\omega) = \Im[W_0^+(\omega)]$ what can be directly proven by use of the identity

$$\delta(\omega' - \omega) = \lim_{\epsilon \searrow 0} \frac{1}{\pi} \frac{\epsilon}{(\omega' - \omega)^2 + \epsilon^2}. \quad (\text{A10})$$

For the next step we look at the transformed Hamiltonian (7) to derive

$$\ddot{q} = -\frac{\partial V}{\partial q} + \lambda_0 X_1 - \delta\Omega_0^2, \quad (\text{A11})$$

$$\ddot{X}_1 = -\Omega_1^2 X_1 + \lambda_0 q + \sum_k C_k X_k, \quad (\text{A12})$$

$$\ddot{X}_k = -\Omega_k^2 X_k^2 + C_k X_1. \quad (\text{A13})$$

Playing the same game as above we can deduce that the Fourier space propagator for the system coordinate is

$$\hat{L}_0(z) = -z^2 - \frac{\lambda_0^2}{\Omega_1^2 - z^2 - W_1(z)} + \delta\Omega_0^2 \quad (\text{A14})$$

which must be the same as Eq. (A7). Furthermore, $W_1(z)$ is defined analogously to Eq. (A8) with $J_0(\omega)$ replaced by $J_1(\omega)$. Then, by comparison with Eq. (A7) we see that

$$W_0(z) = \frac{\lambda_0^2}{\Omega_1^2 - z^2 - W_1(z)}. \quad (\text{A15})$$

Rearranging terms we obtain

$$W_1(z) = \Omega_1^2 - z^2 - \frac{\lambda_0^2}{W_0(z)} \quad (\text{A16})$$

from which we can directly deduce the relation (12). Furthermore, by noting that $W_i(0) = \delta\Omega_i^2$ ($i = 0, 1$) we can also directly verify Eq. (15).

Appendix B: ME without secular approximation for application I

We here provide details for the derivation of the Born-Markov ME based on the system Hamiltonian H'_S (39), which treats the system-RC coupling non-perturbatively while we are aiming at a perturbative treatment of the coupling to the remaining reservoirs. The coupling Hamiltonian is

$$H_I = \sum_{\nu} H_I^{(\nu)} = \sum_{\nu} s_{\nu} \otimes B_{\nu} \quad (\text{B1})$$

with s_h and s_w given in Eqs. (32) and (34) and $s_c = X_1$ due to the RC mapping. Furthermore, for $\nu \in \{h, w\}$ the coupling operators of the bath are $B_{\nu} = -\sum_k c_{k\nu} x_{k\nu}$ and the free bath Hamiltonian reads $H_B^{(\nu)} = \frac{1}{2} \sum_k (p_{k\nu}^2 + \omega_{k\nu}^2 x_{k\nu}^2)$. For $\nu = c$ the form of the operators remains the same but we have to substitute $x_{kc} \rightarrow X_{kc}$, $p_{kc} \rightarrow P_{kc}$, $c_{kc} \rightarrow C_{kc}$ and $\omega_{kc} \rightarrow \Omega_{kc}$.

Note that we are here neglecting renormalization terms of the form $\frac{1}{2} \sum_k \frac{c_{k\nu}^2}{\omega_{k\nu}^2} s_{\nu}^2$ which are of second order in the system-bath coupling. We will later on neglect any Lamb shift terms as well which are also of second order. This is consistent because the heat flows (25) are itself already of second order in the coupling. The contribution due to the renormalization and Lamb shift terms would then be of fourth order in total, which is beyond the validity of our perturbative approach.

After applying the Born and Markov approximation, the formal starting point of the ME is the second order

equation in the interaction picture⁸ [8, 9, 52]

$$\frac{d}{dt}\tilde{\rho}(t) = -\sum_{\nu} \int_0^{\infty} d\tau \text{tr}_{\nu} \left\{ \tilde{H}_I^{(\nu)}(t) \tilde{H}_I^{(\nu)}(t-\tau) \tilde{\rho}(t) R_0^{(\nu)} - \tilde{H}_I^{(\nu)}(t) \tilde{\rho}(t) R_0^{(\nu)} \tilde{H}_I^{(\nu)}(t-\tau) + h.c. \right\}. \quad (\text{B2})$$

Here, $\tilde{\rho}(t)$ is the density matrix of the supersystem (in the interaction picture) and $R_0^{(\nu)} \sim e^{-\beta_{\nu} H_B^{(\nu)}}$ the equilibrium density matrix of the reservoir. Furthermore, the fact that the ME additively decomposes into contributions from each reservoir ν is due to the fact that $\text{tr}_{\nu} \{H_I^{(\nu)} R_0^{(\nu)}\} = 0$.

After introducing the bath correlation function

$$C_{\nu}(\tau) \equiv \text{tr}_{\nu} \left\{ \tilde{B}_{\nu}(\tau) B_{\nu} R_0^{(\nu)} \right\}, \quad (\text{B3})$$

the ME (B2) can be expressed as

$$\begin{aligned} \frac{d}{dt}\tilde{\rho}(t) = & -\sum_{\nu} \int_0^{\infty} d\tau \\ & \times \{C_{\nu}(\tau) [\tilde{s}_{\nu}(t) \tilde{s}_{\nu}(t-\tau) \tilde{\rho}(t) - \tilde{s}_{\nu}(t-\tau) \tilde{\rho}(t) \tilde{s}_{\nu}(t)] \\ & + C_{\nu}^*(\tau) [\tilde{\rho}(t) \tilde{s}_{\nu}(t-\tau) \tilde{s}_{\nu}(t) - \tilde{s}_{\nu}(t) \tilde{\rho}(t) \tilde{s}_{\nu}(t-\tau)]\}. \end{aligned} \quad (\text{B4})$$

If we split the correlation function into real and imaginary part, $C_{\nu}(\tau) = \Re C_{\nu}(\tau) + i\Im C_{\nu}(\tau)$, we can write

$$\begin{aligned} \frac{d}{dt}\tilde{\rho}(t) = & -\sum_{\nu} \int_0^{\infty} d\tau \Re C_{\nu}(\tau) [\tilde{s}_{\nu}(t), [\tilde{s}_{\nu}(t-\tau), \tilde{\rho}(t)]] \\ & - i \sum_{\nu} \int_0^{\infty} d\tau \Im C_{\nu}(\tau) [\tilde{s}_{\nu}(t), \{\tilde{s}_{\nu}(t-\tau), \tilde{\rho}(t)\}]. \end{aligned} \quad (\text{B5})$$

Because

$$\begin{aligned} C_{\nu}(\tau) & \\ & = \sum_k \frac{c_{k\nu}^2}{2\omega_{k\nu}} \{ [1 + n_{\nu}(\omega_{k\nu})] e^{-i\omega_{k\nu}\tau} + n_{\nu}(\omega_{k\nu}) e^{i\omega_{k\nu}\tau} \} \\ & = \frac{1}{\pi} \int_0^{\infty} d\omega J^{(\nu)}(\omega) \{ [1 + n_{\nu}(\omega)] e^{-i\omega\tau} + n_{\nu}(\omega) e^{i\omega\tau} \}, \end{aligned} \quad (\text{B6})$$

we obtain

$$\Re C_{\nu}(\tau) = \frac{1}{\pi} \int_0^{\infty} d\omega J^{(\nu)}(\omega) \cos(\omega\tau) \coth \frac{\beta_{\nu}\omega}{2}, \quad (\text{B7})$$

$$\Im C_{\nu}(\tau) = -\frac{1}{\pi} \int_0^{\infty} d\omega J^{(\nu)}(\omega) \sin(\omega\tau). \quad (\text{B8})$$

Here, we used that $1 + 2n_{\nu}(\omega) = \coth \frac{\beta_{\nu}\omega}{2}$. Finally, after leaving the interaction picture the ME (B5) becomes

$$\begin{aligned} \frac{d}{dt}\rho(t) = & -i[H'_S, \rho(t)] \\ & - \sum_{\nu} \int_0^{\infty} d\tau \Re C_{\nu}(\tau) [s_{\nu}, [\tilde{s}_{\nu}(-\tau), \rho(t)]] \\ & - i \sum_{\nu} \int_0^{\infty} d\tau \Im C_{\nu}(\tau) [s_{\nu}, \{\tilde{s}_{\nu}(-\tau), \rho(t)\}]. \end{aligned} \quad (\text{B9})$$

This form is still not very useful for numerical implementation. To achieve this goal we write

$$s_{\nu}(-\tau) = \sum_{kl} s_{\nu}^{kl} e^{-i\omega_{kl}\tau} |k\rangle\langle l| \quad (\text{B10})$$

with $H'_S |k\rangle = E_k |k\rangle$ and $\omega_{kl} \equiv E_k - E_l$. Upon using the identity

$$\int_0^{\infty} d\tau e^{\pm i\omega\tau} = \pi\delta(\omega) \pm i\mathcal{P}\frac{1}{\omega}, \quad (\text{B11})$$

and neglecting the principal value (Lamb shift) terms, we arrive at a ME of the form

$$\begin{aligned} \frac{d}{dt}\rho(t) = & -i[H'_S, \rho(t)] \\ & - \sum_{\nu} [s_{\nu}, [\chi_{\nu}, \rho(t)]] + \sum_{\nu} [s_{\nu}, \{\Theta_{\nu}, \rho(t)\}]. \end{aligned} \quad (\text{B12})$$

The new operators appearing in this equation are given as

$$\chi_{\nu} = \frac{1}{2} \sum_{kl} J^{(\nu)}(\omega_{kl}) \coth \frac{\beta_{\nu}\omega_{kl}}{2} s_{\nu}^{kl} |k\rangle\langle l|, \quad (\text{B13})$$

$$\Theta_{\nu} = \frac{1}{2} \sum_{kl} J^{(\nu)}(\omega_{kl}) s_{\nu}^{kl} |k\rangle\langle l|. \quad (\text{B14})$$

Finally, the model is specified by choosing the SDs of the baths as discussed in the main text. For the work bath we again use $J^{(w)}(\omega) = J_0^{(w)}(\omega) = \beta_w \Delta_{10} \Gamma_w$ to mimic a constant SD in the infinite temperature limit. The SD of the hot bath is parameterized by $J^{(h)}(\omega) = J_0^{(h)}(\omega) = \frac{\Gamma_h \omega}{\Delta_{20}} \Theta(\omega_R - \omega)$ and for the cold bath $J^{(c)}(\omega) = J_1^{(c)}(\omega)$ is given by the relation (12) with $J_0^{(c)}(\omega)$ given in Eq. (37). We are especially interested in the regime of a large cutoff frequency $\omega_R \gg 1$ because this allows by virtue of the residue theorem to evaluate $J_1^{(c)}(\omega)$ exactly.⁹ Then, for $4\omega_0^2 > \gamma^2$, it follows that

$$J_1^{(c)}(\omega) = \gamma\omega\Theta(\omega_R - \omega). \quad (\text{B15})$$

⁸ The interaction picture is defined by $\tilde{A}(t) \equiv e^{+i(H'_S + H_B)t} A e^{-i(H'_S + H_B)t}$.

⁹ The residue theorem requires $J_0(\omega)$ to be analytic (except for isolated poles), which is – strictly speaking – never the case for a hard cutoff $\Theta(\omega_R - \omega)$. However, the discrepancy with the true solution vanishes for $\omega_R \rightarrow \infty$.

Furthermore, we also have $\lambda_0 = d_0$ and $\delta\Omega_0 = d_0/\omega_0$ such that the frequency of the RC is $\frac{\lambda_0}{\delta\Omega_0} = \omega_0$.

The secular ME requires to perform an additional approximation on top of the Born-Markov ME (B12). This can be done by averaging the generator of the Born-Markov ME in the interaction picture in time (similar to a rotating wave approximation) [6, 52] or by dynamical coarse graining of the time-evolution [9, 75]. We will skip any details here because the secular ME is also reviewed in Appendix C.

Appendix C: BMS ME for application II

For a non-degenerate system Hamiltonian, it is well-known that the BMS ME yields a simple rate equation (“Pauli ME”) in the eigenbasis of H_S [4, 9, 52]. This can be put into the form

$$\dot{P}_k = \sum_l W_{kl} P_l, \quad (\text{C1})$$

where P_k is the probability to find the system in state $|k\rangle$ and the transition rate from energy eigenstate l to k is given by

$$W_{kl} = \sum_{\alpha\beta} \gamma_{\alpha\beta} (E_l - E_k) \langle k | A_\beta | l \rangle \langle k | A_\alpha^\dagger | l \rangle^*. \quad (\text{C2})$$

Here, we assumed a general interaction Hamiltonian of the form $H_I = \sum_\alpha A_\alpha \otimes B_\alpha$. Furthermore, the $\gamma_{\alpha\beta}$ denote the Fourier transforms of the reservoir correlation functions

$$\gamma_{\alpha\beta}(\omega) = \int_{-\infty}^{\infty} d\tau \text{tr}_B \{ B_\alpha(\tau) B_\beta R_0 \} e^{+i\omega\tau}. \quad (\text{C3})$$

For our model from Sec. V, we identify the coupling operators

$$A_1 = d, \quad B_1 = \sum_k t_{kL} c_{kL}^\dagger, \quad (\text{C4})$$

$$A_2 = d^\dagger, \quad B_2 = \sum_k t_{kL}^* c_{kL}, \quad (\text{C5})$$

$$A_3 = d, \quad B_3 = \sum_k t_{kR} c_{kR}^\dagger, \quad (\text{C6})$$

$$A_4 = d^\dagger, \quad B_4 = \sum_k t_{kR}^* c_{kR}, \quad (\text{C7})$$

$$A_5 = \frac{1}{\sqrt{2\Omega_1}} (a_1 + a_1^\dagger), \quad (\text{C8})$$

$$B_5 = -\sum_q \frac{C_q}{\sqrt{2\Omega_q}} (a_q + a_q^\dagger), \quad (\text{C9})$$

and the non-vanishing correlation functions yield

$$\gamma_{12}(\omega) = \Gamma_L(-\omega) f_L(-\omega), \quad (\text{C10})$$

$$\gamma_{21}(\omega) = \Gamma_L(+\omega) [1 - f_L(+\omega)], \quad (\text{C11})$$

$$\gamma_{34}(\omega) = \Gamma_R(-\omega) f_R(-\omega), \quad (\text{C12})$$

$$\gamma_{43}(\omega) = \Gamma_R(+\omega) [1 - f_R(+\omega)], \quad (\text{C13})$$

$$\gamma_{55}(\omega) = J_1(+\omega) [1 + n_B(+\omega)]. \quad (\text{C14})$$

Here, we have used the definition of the fermionic SD (56) and the SD of the residual oscillators is as usual defined by

$$J_1(\omega) = \frac{\pi}{2} \sum_q \frac{C_q^2}{\Omega_q} \delta(\omega - \Omega_q). \quad (\text{C15})$$

From Eq. (C2) and Eqs. (C10) to (C14) we see that the rates additively decompose into left, right, and phonon contributions and the total rate matrix in Eq. (C1) has the structure $W = W^L + W^R + W^{\text{ph}}$, where for $k \neq l$ we have

$$W_{kl}^L = \gamma_{12} (E_l - E_k) |\langle k | d^\dagger | l \rangle|^2 + \gamma_{21} (E_l - E_k) |\langle k | d | l \rangle|^2, \quad (\text{C16})$$

$$W_{kl}^R = \gamma_{34} (E_l - E_k) |\langle k | d^\dagger | l \rangle|^2 + \gamma_{43} (E_l - E_k) |\langle k | d | l \rangle|^2, \quad (\text{C17})$$

$$W_{kl}^{\text{ph}} = \gamma_{55} (E_l - E_k) \frac{1}{2\Omega_1} \left| \langle k | (a_1 + a_1^\dagger) | l \rangle \right|^2. \quad (\text{C18})$$

To make the transition rates explicit, we have to evaluate the matrix elements of the system coupling operators, too. The electronic jumps can be separated into pure electronic transitions and bosonic excitations of the RC. Denoting by $|\widetilde{n}', m'\rangle \equiv U|n, m\rangle$ the basis in the original frame, we obtain

$$\begin{aligned} |\langle n', m' | A_1 | n, m \rangle|^2 &= \left| \langle \widetilde{n}', \widetilde{m}' | d e^{-\frac{\lambda}{\Omega_1} (a_1 - a_1^\dagger)} | \widetilde{n}, \widetilde{m} \rangle \right|^2 \\ &= \delta_{n',0} \delta_{n,1} \left| \langle \widetilde{m}' | e^{-\frac{\lambda}{\Omega_1} (a_1 - a_1^\dagger)} | \widetilde{m} \rangle \right|^2, \end{aligned} \quad (\text{C19})$$

$$|\langle n', m' | A_2 | n, m \rangle|^2 = \delta_{n',1} \delta_{n,0} \left| \langle \widetilde{m}' | e^{+\frac{\lambda}{\Omega_1} (a_1 - a_1^\dagger)} | \widetilde{m} \rangle \right|^2, \quad (\text{C20})$$

whereas the transitions triggered by the phonon reservoir simply yield

$$\begin{aligned} |\langle n', m' | A_5 | n, m \rangle|^2 &= \frac{\delta_{n,n'}}{2\Omega_1} \left| \langle \widetilde{m}' | (a_1 + a_1^\dagger) | \widetilde{m} \rangle \right|^2 \\ &= \frac{\delta_{n,n'}}{2\Omega_1} [\delta_{m',m+1} (m+1) + \delta_{m',m-1} m]. \end{aligned} \quad (\text{C21})$$

Having the rates at hand, we are now finally able to compute the quantities shown in Sec. V C. A visualization of the resulting rate equation, which has a highly connected structure, is also provided in Fig. 8.